X-690-71-449
PREPRINT

NASA TM X- 65767

MAGNETIC FIELD MEASUREMENTS BY PIONEER 6

I. Hourly Averages of the Field Elements from 17 December 1965 to 5 September 1967 (Bartels' Solar Rotation 1811 to 1834)

NORMAN F. NESS
FRANKLIN W. OTTENS

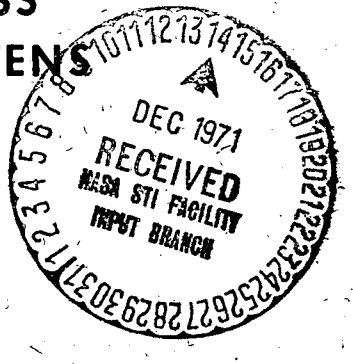

NOVEMBER 1971

GODDARD SPACE FLIGHT CENTER
GREENBELT, MARYLAND

X-690-71-449

MAGNETIC FIELD MEASUREMENTS BY PIONEER 6

I. Hourly averages of the field elements from 17 December 1965 to 5 September 1967 (Bartels' Solar Rotation 1811 to 1834).

Norman F. Ness
Franklin W. Ottens

Laboratory for Extraterrestrial Physics
NASA-Goddard Space Flight Center
Greenbelt, Maryland USA 20771

November 1971

1. Introduction

The Pioneer 6 spacecraft is a spin stabilized interplanetary probe launched from the Eastern Test Range, Cape Kennedy, Florida on 16 December 1965. The geocentric orbit of the spacecraft has an aphelion of 0.987 AU, a perihelion 0.814 AU, inclination to the ecliptic of 0.2° and orbital period of 311 days. This spacecraft was the first of a series of four Pioneer spacecraft with identical structures but slightly different complements of experiments. A NASA-GSFC magnetic field experiment was proposed, accepted and flown on Pioneers 6 and 7 (in 1966). Subsequently, unique circumstances presented an opportunity for flight of a similar experiment by the GSFC group in collaboration with the University of Rome, Laboratory for Space Plasma Research group on Pioneer 8 (in 1967).

The magnetic field experiment detector is a monoaxial fluxgate magnetometer sensor mounted on the end of a boom at a distance of 2.1 meters from the spacecraft spin axis. The initial spin period was approximately one second and the field measurements were synchronized with the rotation of the spacecraft. The monoaxial sensor was oriented at an angle of 54° 45' to the spin axis so that during one spacecraft rotation three samples of the magnetic field at equal intervals yielded three independent measurements in mutually orthogonal directions. These basic measurements, obtained in a time interval of 2/3 of a second, define the total vector magnetic field in a spacecraft coordinate system.

The spin axis of the spacecraft was oriented orthogonal to the ecliptic plane with the high gain antenna of the spacecraft pointing to the south ecliptic pole.

Data transmission from the spacecraft experiment was synchronized with telemetry, which ranged from 8 to 512 bits/sec during the lifetime of the spacecraft. A complete three component measurement was not read out during each spin period and so individual data points are not equally spaced in time (see Scearce et al., 1968 for description of the experiment).

The Pioneer 6 instrument was a single range magnetometer ($\pm 64\gamma$) which with the 8 bit quantization of the analog to digital converter yielded a digital window size of $\pm 0.25\gamma$. The RMS noise level of the sensor was 0.12γ and the bandwidth 0 to 5 cps. The magnetic field of the spacecraft and associated solar array as measured at the sensor location was estimated to be less than 0.3γ. Periodic sensitivity calibrations were made once each day as well as zero level checks approximately once every several months. Pioneer 6 carried the first device to check the zero-level of a fluxgate magnetometer sensor inflight. The projection of the orbit described by Pioneer 6 on the ecliptic plane relative, to the earth-sun-line, is shown in Figure 1.

2. Data

The magnetic field elements have been computed in a spacecraft centered solar ecliptic system in which the X axis points from the spacecraft to the sun, the Z axis to the ecliptic north pole and the Y axis being the third axis of the orthogonal right handed coordinate system.

The standard data analysis was performed to yield 30 second averages of the field components and the field magnitudes as

$$\bar{X} = \frac{1}{n} \sum_{i=1}^{n} X_i \text{ etc.}, \quad \bar{F} = \frac{1}{n} \sum_{i=1}^{n} F_i, \quad \bar{\bar{F}} = \sqrt{(\bar{X})^2+(\bar{Y})^2+(\bar{Z})^2} \qquad (1)$$

Also RMS deviations $(\delta_X, \delta_Y, \delta_Z)$ of the magnetic field were computed routinely for each component and for the field magnitude. The Pythagorean variance, which is an invarient of the coordinate system, is obtained from the component deviations as

$$\delta = \sqrt{\delta_X^2 + \delta_Y^2 + \delta_Z^2} \qquad (2)$$

The choice of a 30 second time interval was based upon a desire to provide correlative data to each of the plasma probes on the Pioneer 6 and 7 spacecraft whose fastest cycle times were on the order of one minute.

Data shown in Figures 2 through 22 represent for each solar rotation the hourly averages of the field elements $\bar{F}$, $\bar{\bar{F}}$, θ (latitude) and ϕ (longitude). The data are plotted in 27 day increments corresponding to Bartels' solar

rotation numbering system. The two variances D_1 and D_2 are obtained by different means. D_1 is a variance computed from equation 2 for each hourly interval using the hourly averaged components (and deviations from them). D_2 is the hourly average of the individual Pythagorean variance for each 30 time interval. The days of the year are indicated as calendar days and most of the missing data corresponds to gaps in tracking coverage of the spacecraft. Publications utilizing Pioneer 6 data which have already appeared are given in the reference list. This does not include those publications by other non-GSFC associated authors who have used Pioneer 6 data.

3. Summary

The most important scientific discoveries of the Pioneer 6 magnetic field experiment have related to the microstructure of the interplanetary medium as well as the large scale structure of the interplanetary magnetic field. In addition, correlative studies with the MIT plasma probe have provided further insight into the nature of the microstructure of the interplanetary plasma.

The 30 second average detail data and hourly average data are available from the National Space Science Data Center at NASA-GSFC (Mail Code 601), Greenbelt, Maryland 20771. This present document provides, in summary graphical form, a working data set which was used internally at the NASA-GSFC and parts of which have been made available to other groups.

4. References (in chronological order)

1. Ness, N. F., C. S. Scearce and S. Cantarano, Preliminary Results from the Pioneer VI Magnetic Field Experiment, J. Geophys. Res., 71, 3305-3313, 1966.

2. Ness, Norman F., Simultaneous Measurements of the Interplanetary Magnetic Field, J. Geophys. Res., 71, 3315-3318, 1966.

3. McCracken, K. G., and N. F. Ness, Collimation of Solar Cosmic Rays by the Interplanetary Magnetic Field, J. Geophys. Res., 71, 3319-3324, 1966.

4. Burlaga, Leonard F. and Norman F. Ness, Micro and Macro-Structure of the Interplanetary Magnetic Field, Canadian Journal of Physics, 46, 962-965, 1968.

5. Burlaga, L. F., Microscale Structures in the Interplanetary Medium, Solar Physics, 4, 67, 1968.

6. Burlaga, L. F., Directional Discontinuities in the Interplanetary Magnetic Field, Solar Physics, 7, 54-71, 1969.

7. McCracken, K. G., U. R. Rao and N. F. Ness, The Interrelationship of Cosmic Ray Anisotropies and the Interplanetary Magnetic Field, J. Geophys. Res., 73, 4159-4166, 1968.

8. Ness, N. F., and H. E. Taylor, Observations of the Interplanetary Magnetic Field July 4-12, 1966, Annals IQSY, 1968.

9. Ness, Norman F., Observed Properties of the Interplanetary Plasma, Ann. Revs. Astronomy and Astrophysics, Vol. 6, Ch. 4, ed by Goldberg, Layzer and Phillips, pp. 79-114, 1968.

10. Ness, Norman F., Direct Measurements of Interplanetary Magnetic Field and Plasma, Annals IQSY, Vol. 4, 88-109, 1969.

11. Sari, James and Norman F. Ness, Power Spectra of the Interplanetary Magnetic Field, Solar Physics, 1969.

12. Scearce C. S., C. Ehrmann, S. C. Cantarano and N. F. Ness, Magnetic Field Experiment: Pioneers 6, 7 and 8, NASA-GSFC Preprint X-616-68-370.

13. Burlaga, L. F., and N. F. Ness, Tangential Discontinuities in the Solar Wind, Solar Physics, 9, 467, 1969.

14. Ness, N. F., The Magnetic Structure of Interplanetary Space, Proceedings Budapest XI International Cosmic Ray Conference, 1969, 690-69-334.

15. Sari, J. W., and N. F. Ness, Power Spectral Studies of the Interplanetary Magnetic Field, Proc. Eleventh International Conference on Cosmic Rays, ed. by P. Gombas, pp. 373-378, 1970.

16. Burlaga, L. F., Discontinuities and Shock Waves in the Interplanetary Medium and Their Interaction with the Magnetosphere, International STP Symposium in Leningrad, USSR, May 1970. (Also X692-70-154).

17. Burlaga, L. F., On the Nature and Origin of Directional Discontinuities, J. Geophys. Res., 76, 4360, 1971.

18. Mariani, F., N. F. Ness and J. Chao, Re-Interpretation of the Pioneer 6 Bow Shock Crossing, X-690-71-24.

List of Figures

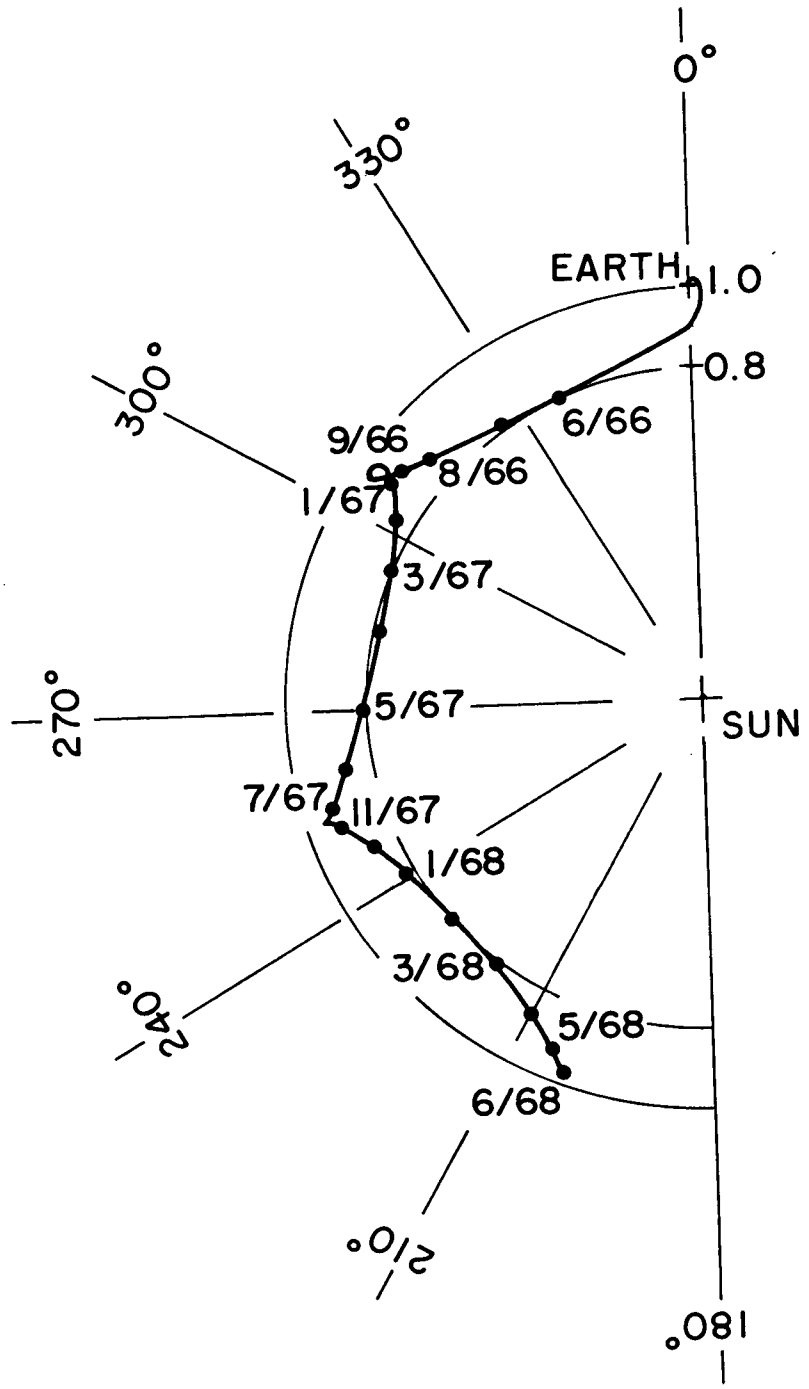
0°
330°
EARTH
1.0
0.8
300°
6/66
9/66
8/66
1/67
3/67
270°
5/67
SUN
7/67
11/67
1/68
3/68
240°
5/68
6/68
210°
180°

FIGURE 1

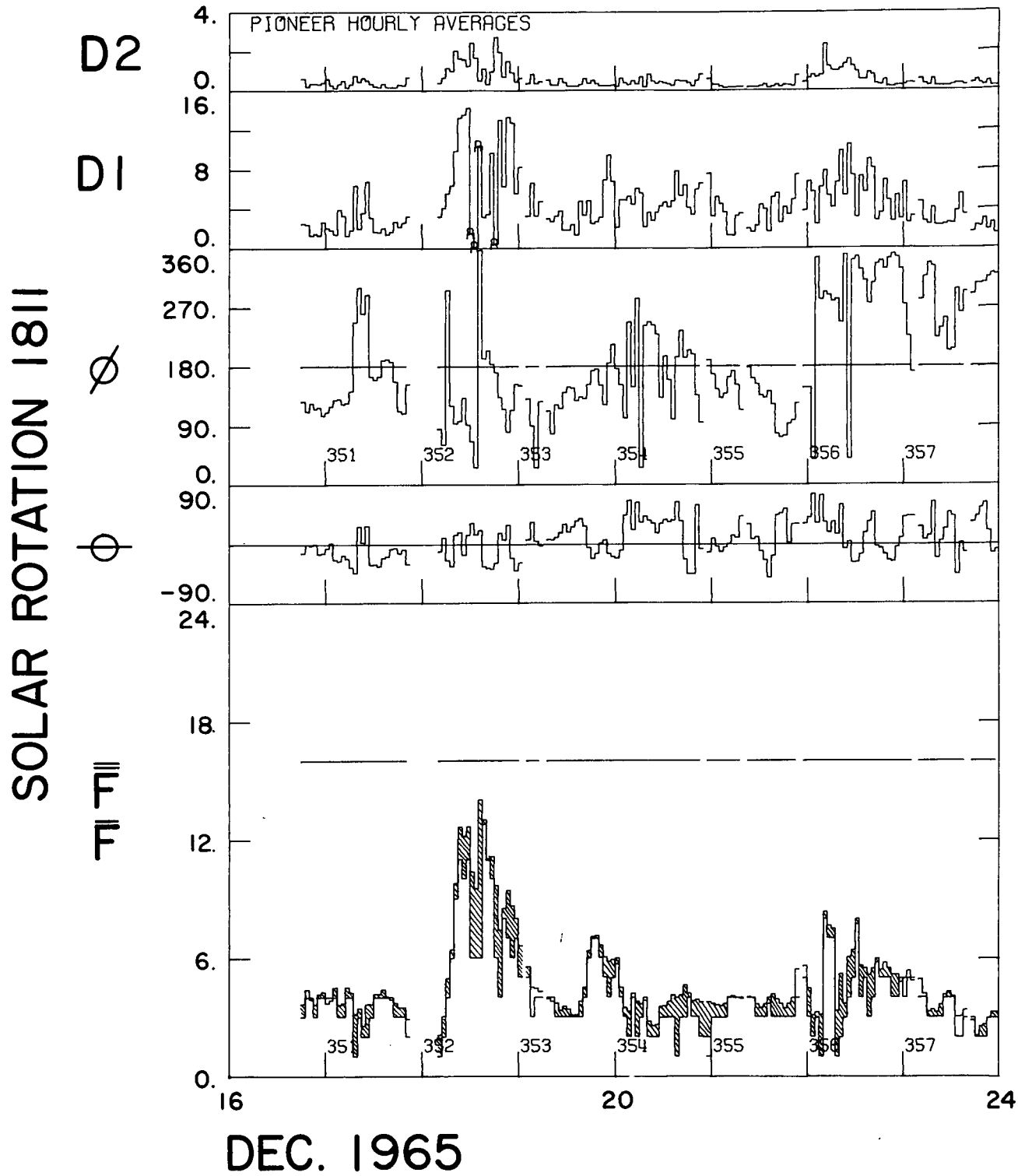
PIONEER HOURLY AVERAGES
D2
4.
0.
D1
16.
8
0.
360.
270.
180.
90.
0.
351
352
353
354
355
356
357
90.
-90.
24.
18.
12.
6.
0.
16
20
24
DEC. 1965
SOLAR ROTATION 1811

FIGURE 2

FOLDOUT FRAME 1

FOLDOUT FRAME 2

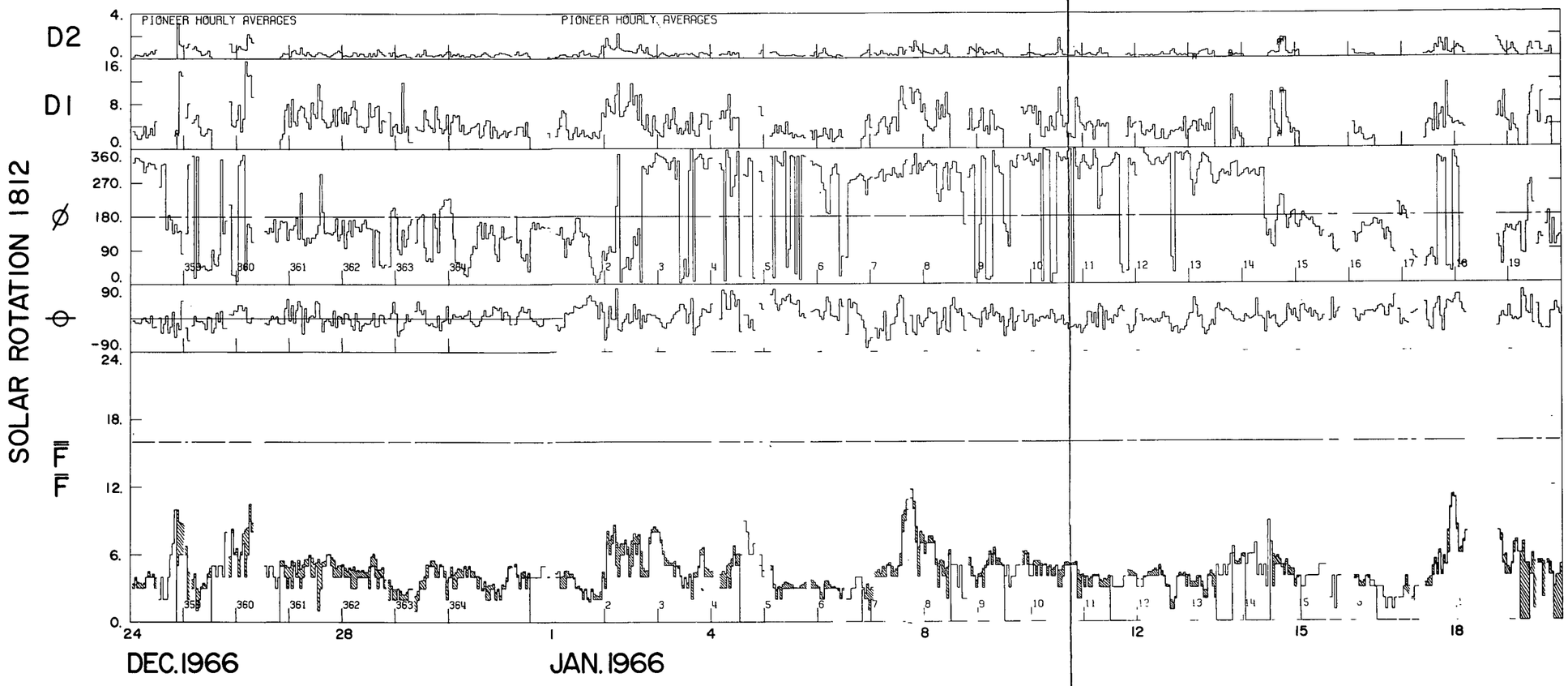

FIGURE 3

FOLDOUT FRAME 1

FOLDOUT FRAME 2

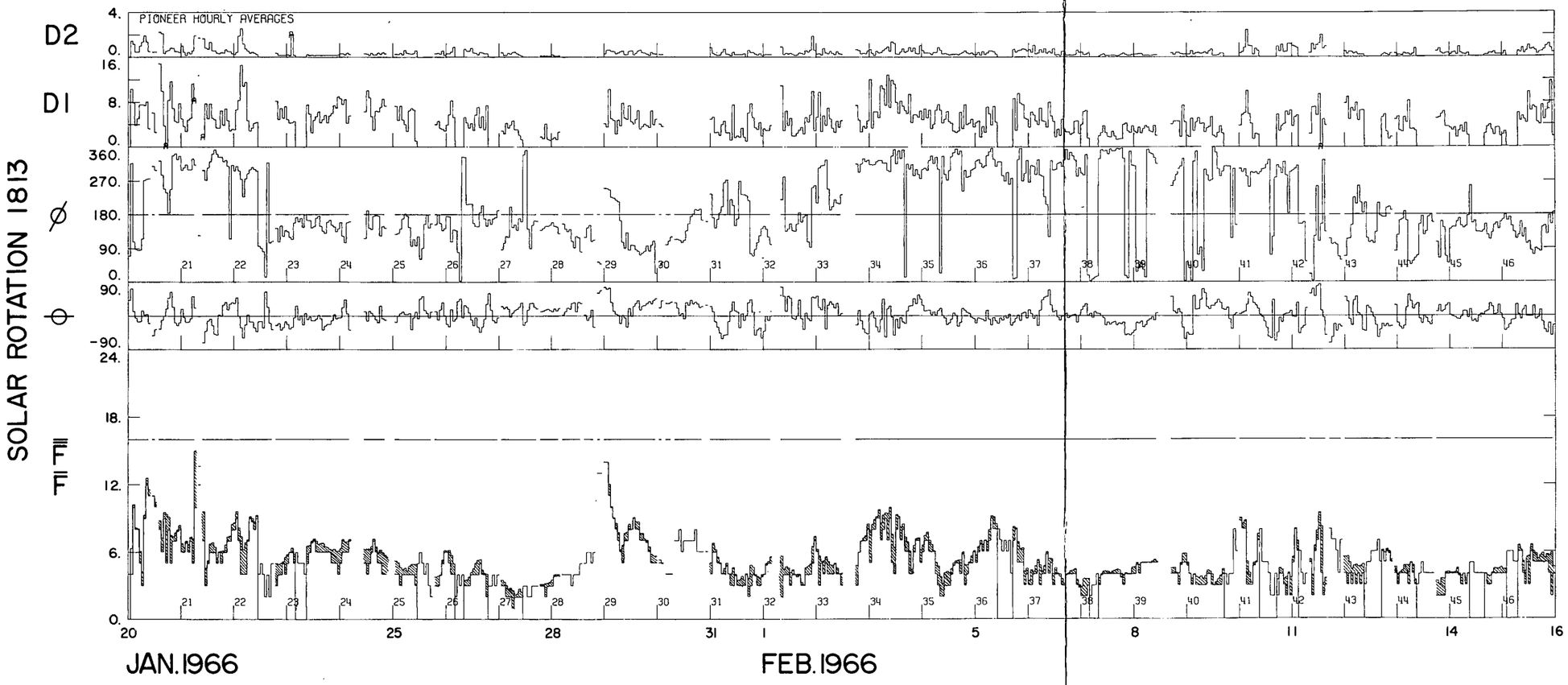

FIGURE 4

FOLDOUT FRAME 1

FOLDOUT FRAME 2

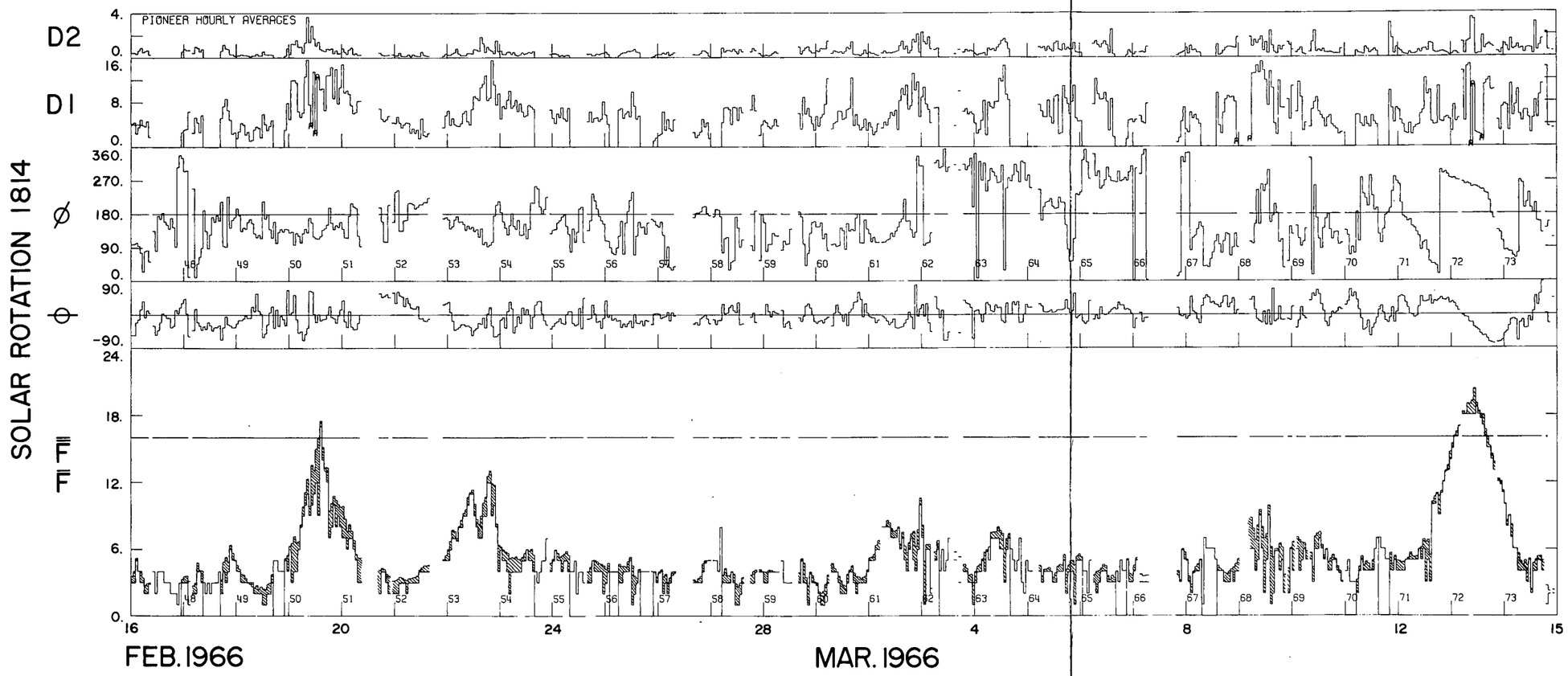

FIGURE 5

FOLDOUT FRAME 1

FOLDOUT FRAME 2

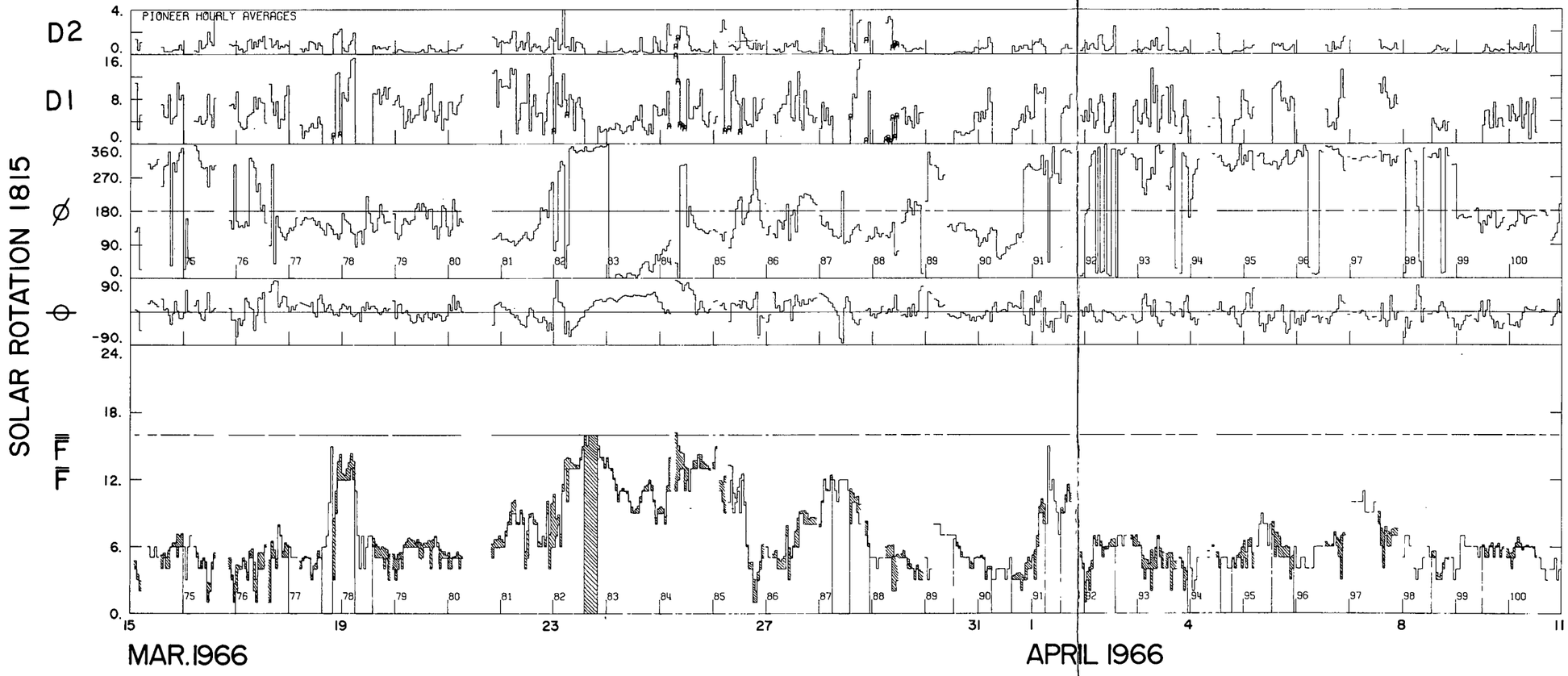

FIGURE 6

FOLDOUT FRAME 1

FOLDOUT FRAME 2

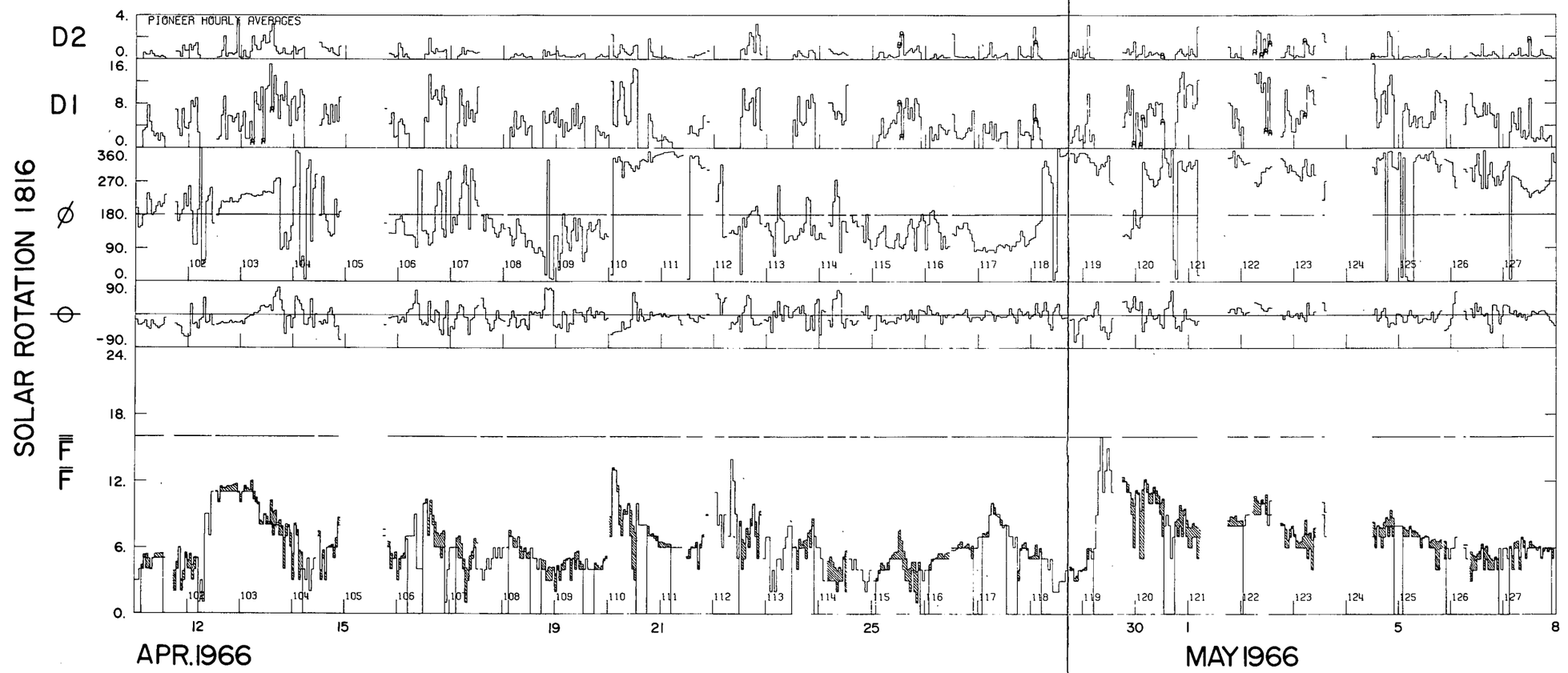

FIGURE 7

FOLDOUT FRAME 1

FOLDOUT FRAME 2

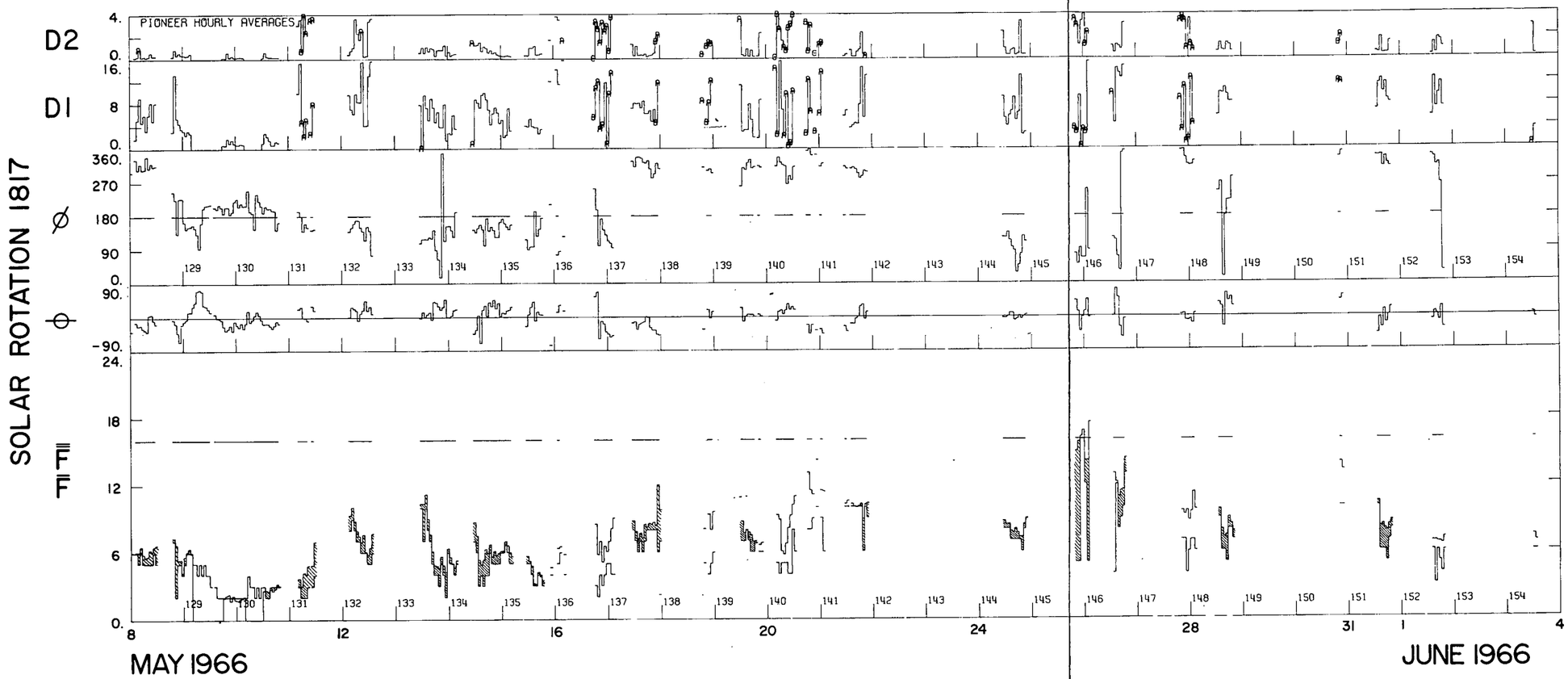

FIGURE 8

FOLDOUT FRAME 1

FOLDOUT FRAME 2

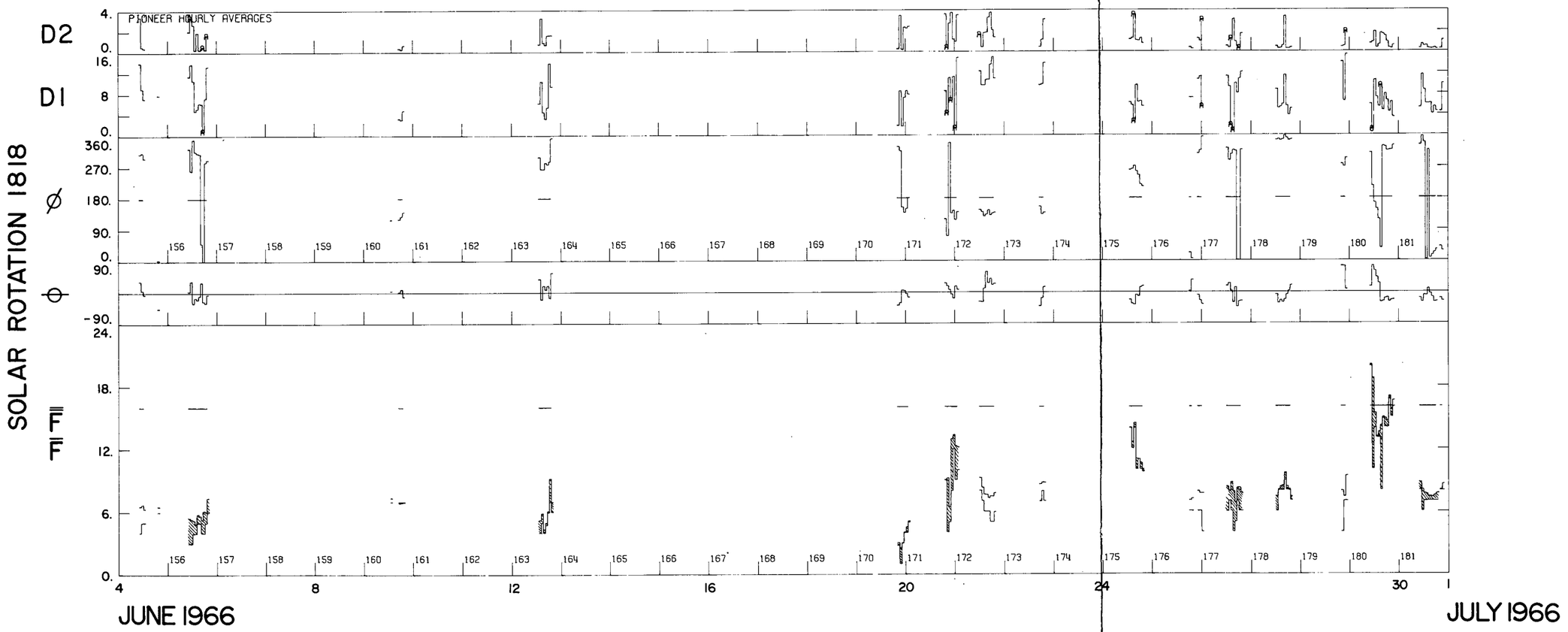

FIGURE 9

FOLDOUT FRAME 1

FOLDOUT FRAME 2

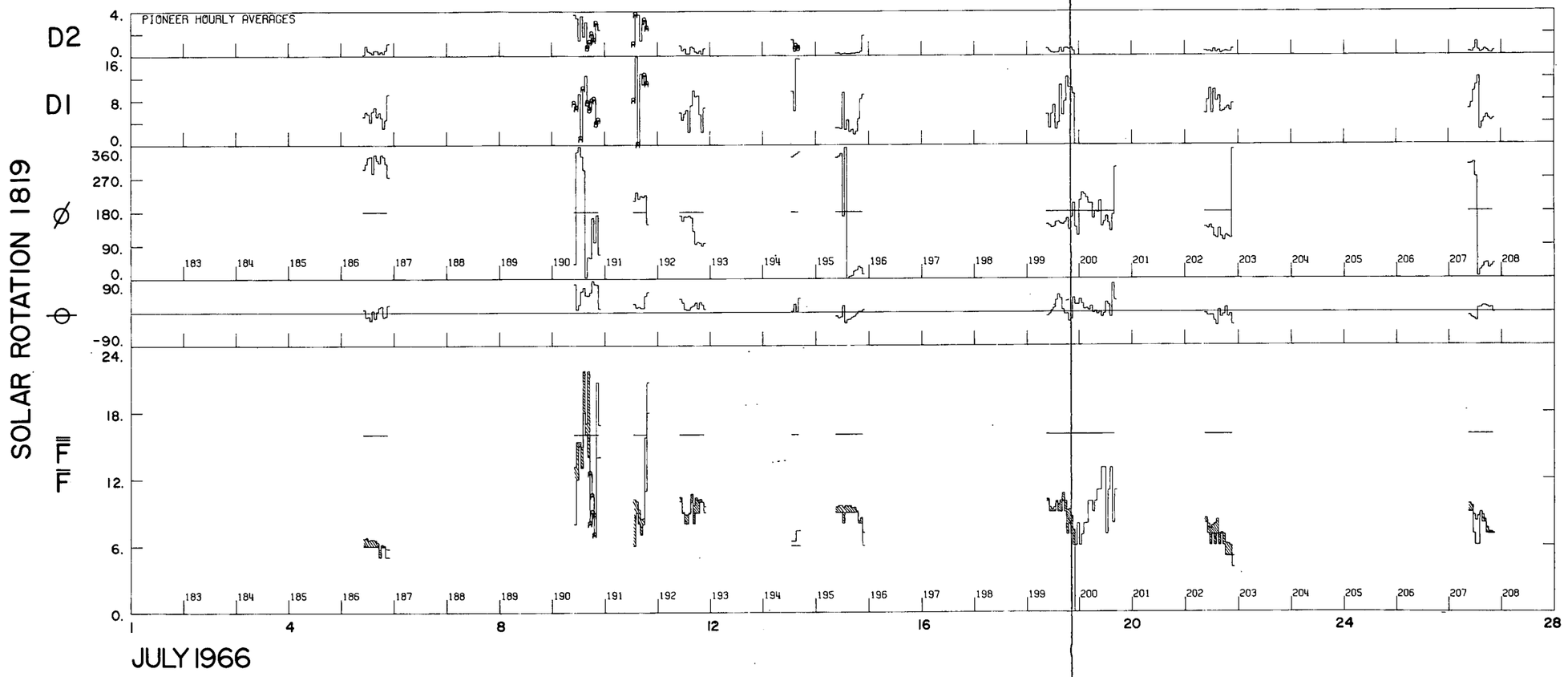

FIGURE 10

FOLDOUT FRAME 1

FOLDOUT FRAME 2

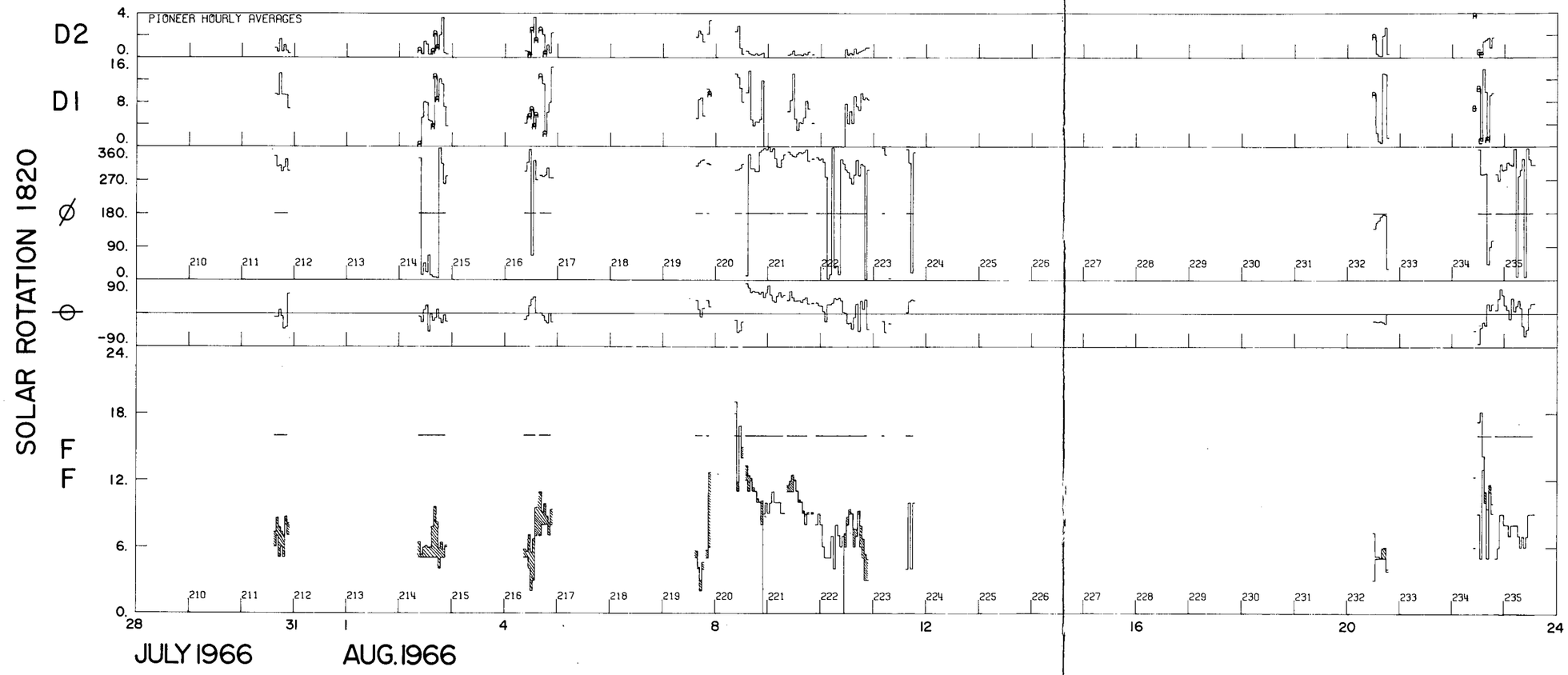

FIGURE 11

FOLDOUT FRAME 1

FOLDOUT FRAME 2

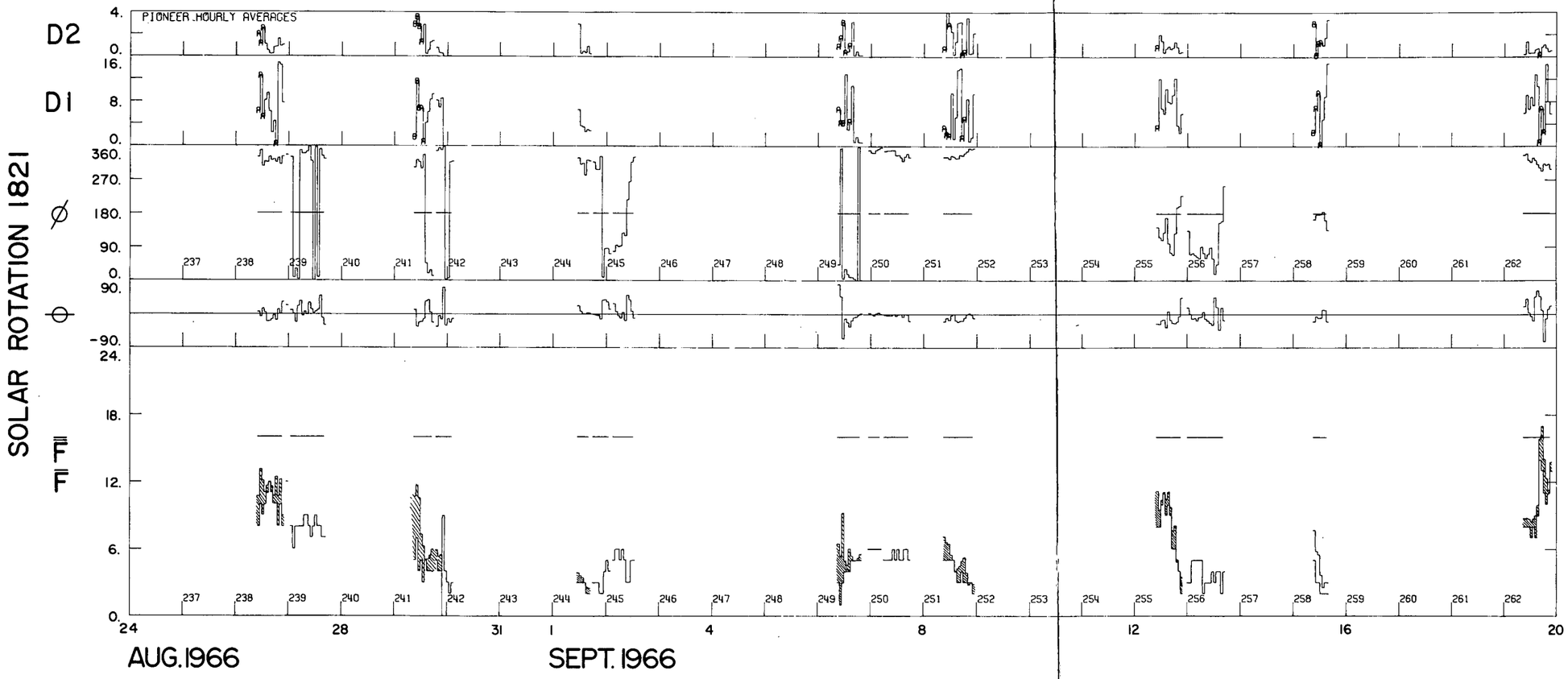

FIGURE 12

FOLDOUT FRAME 1

FOLDOUT FRAME 2

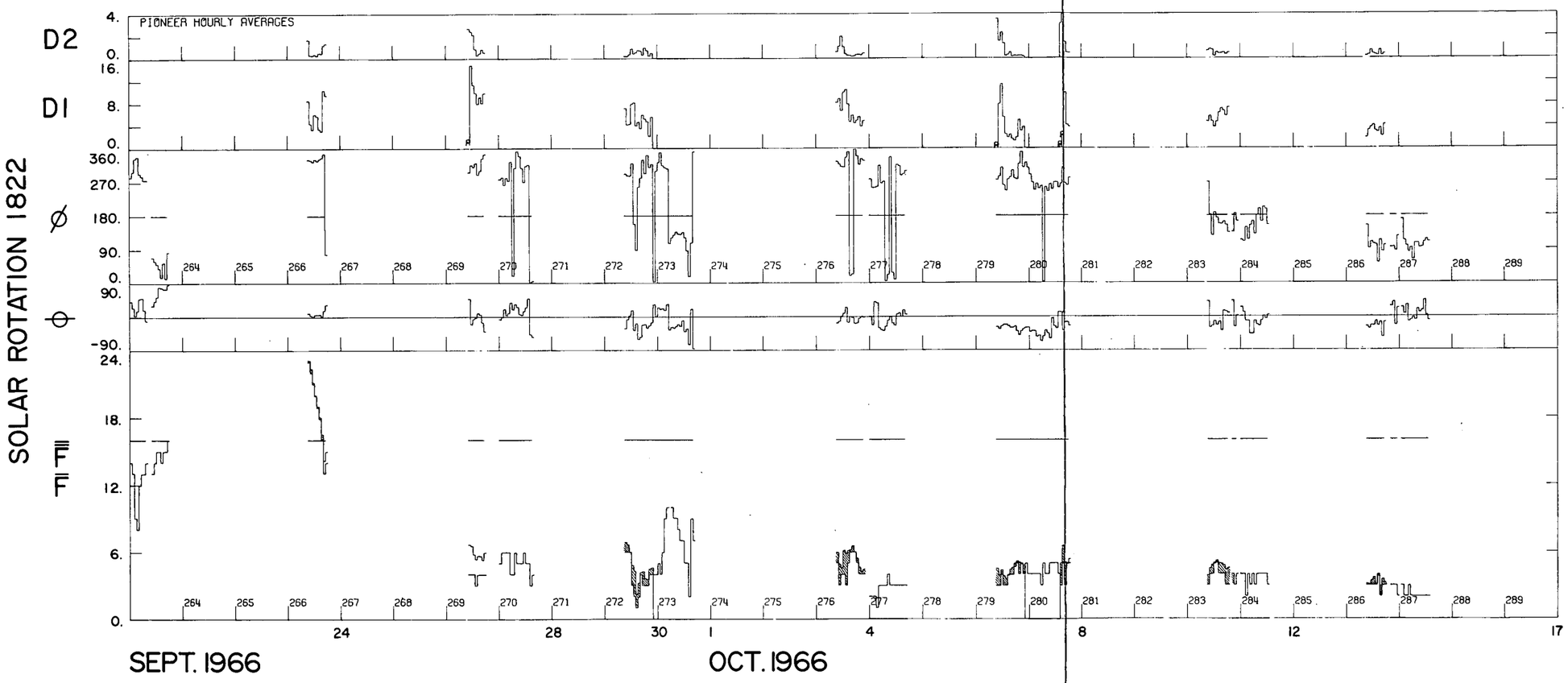

FIGURE 13

FOLDOUT FRAME 1

FOLDOUT FRAME 2

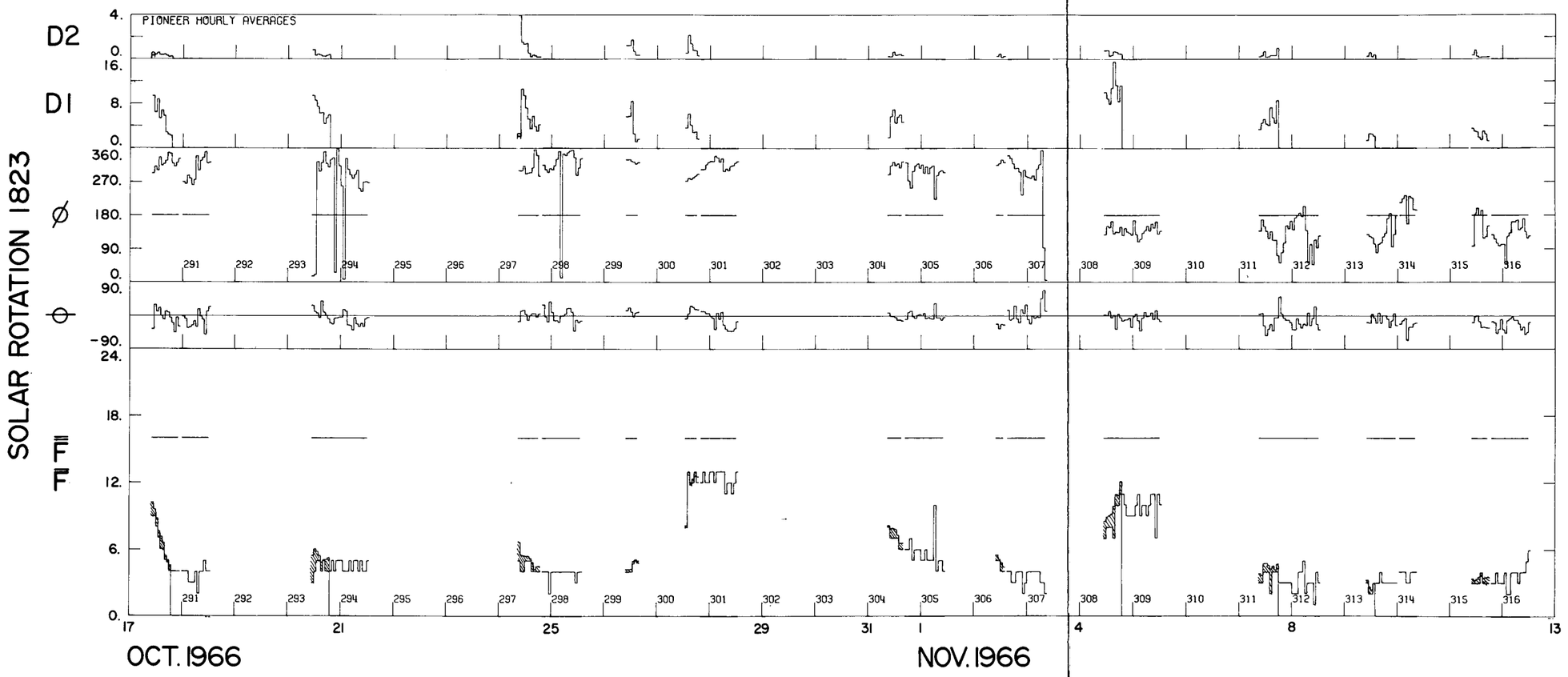

FIGURE 14

FOLDOUT FRAME 1

FOLDOUT FRAME 2

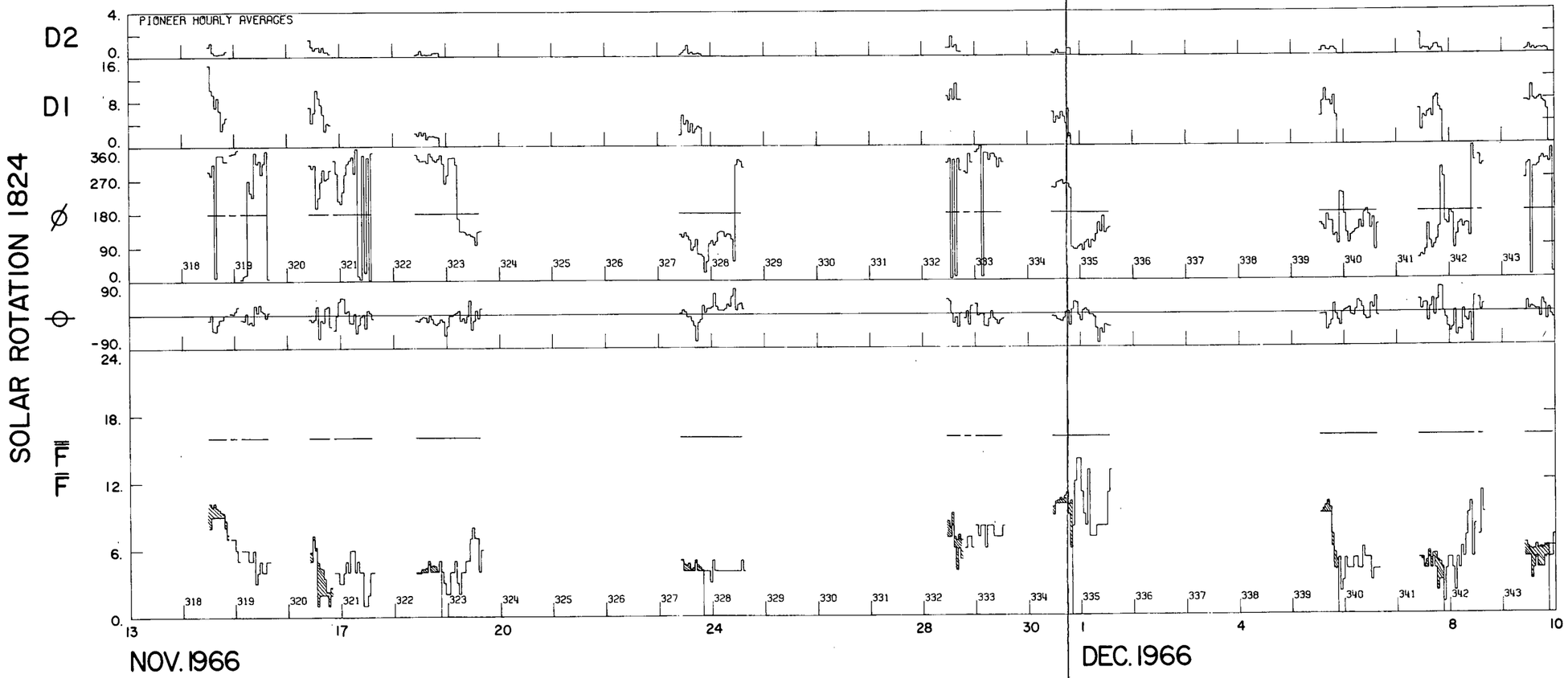

FIGURE 15

FOLDOUT FRAME 1

FOLDOUT FRAME 2

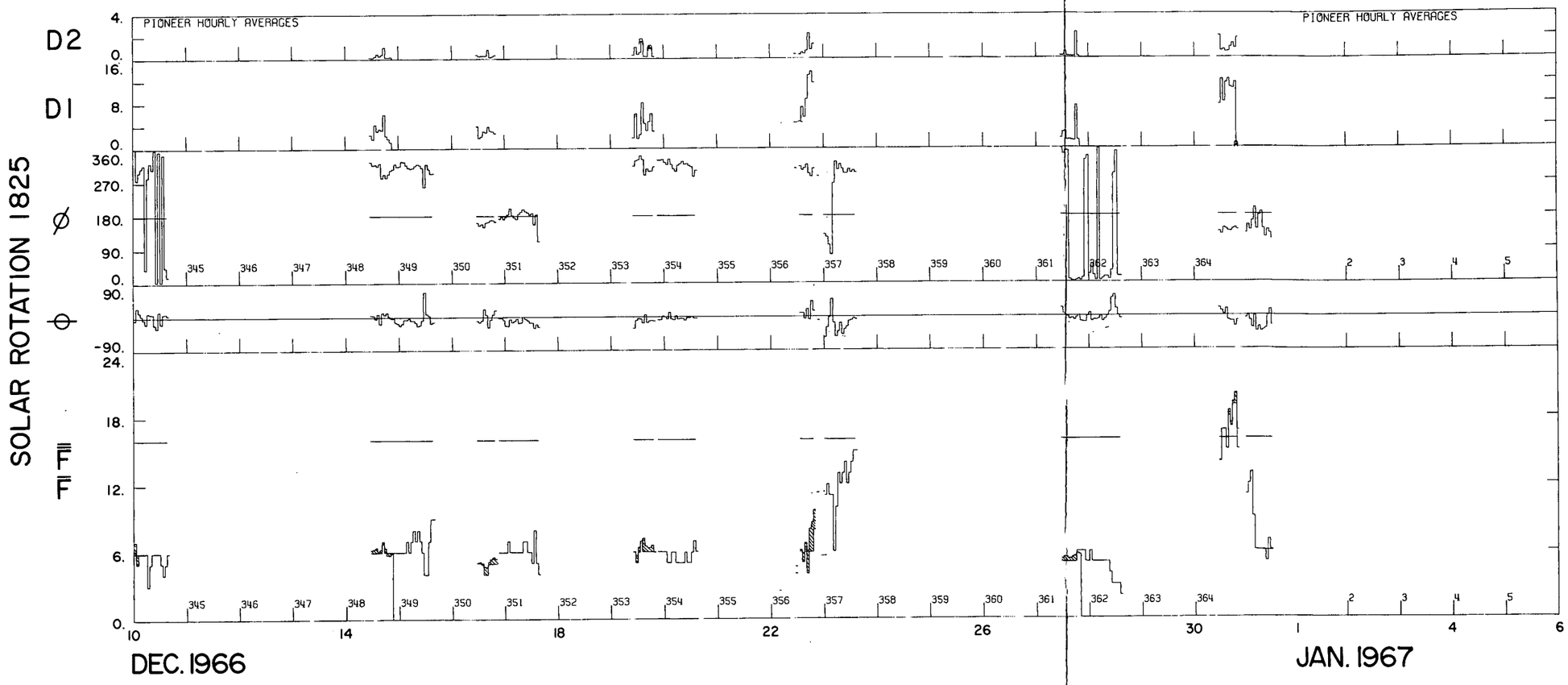

FIGURE 16

FOLDOUT FRAME 1

FOLDOUT FRAME 2

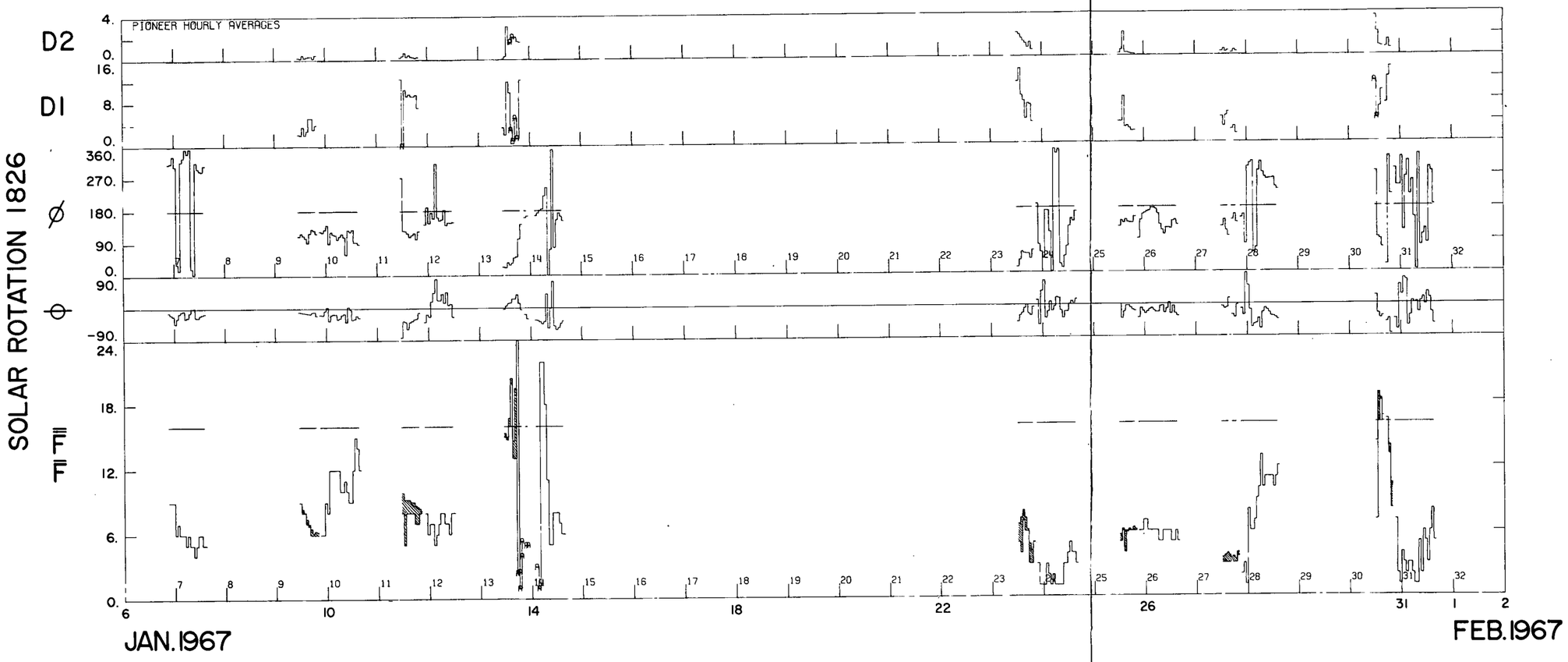

FIGURE 17

FOLDOUT FRAME 1

FOLDOUT FRAME 2

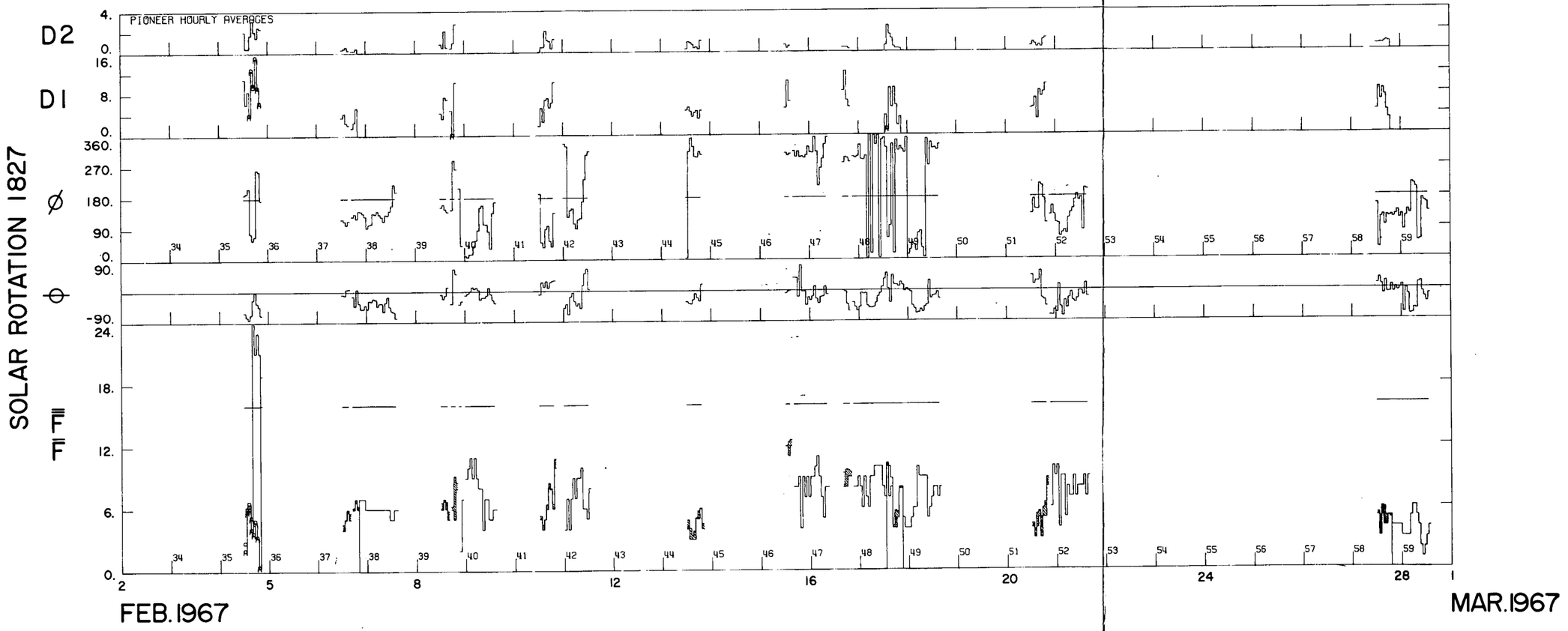

FIGURE 18

FOLDOUT FRAME 1

FOLDOUT FRAME 2

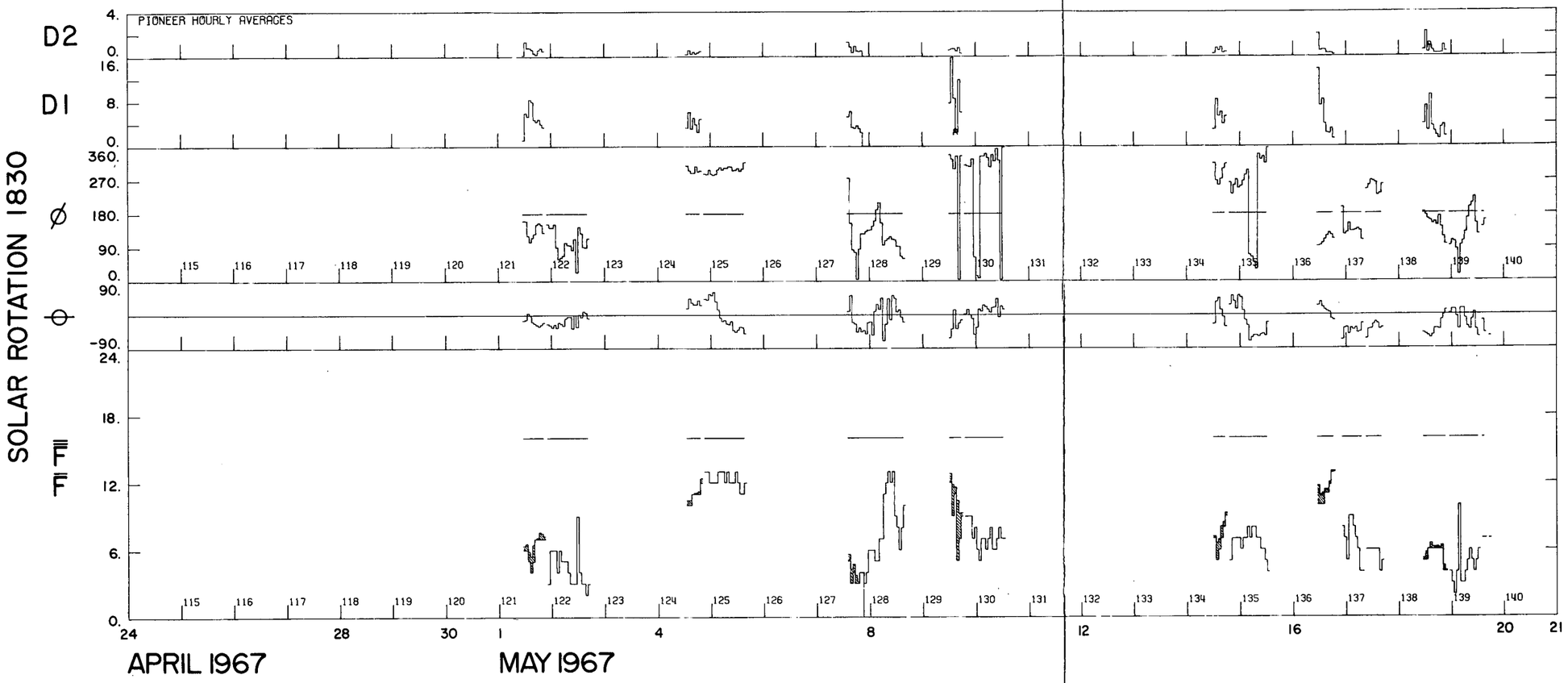

FIGURE 19

FOLDOUT FRAME 1

FOLDOUT FRAME 2

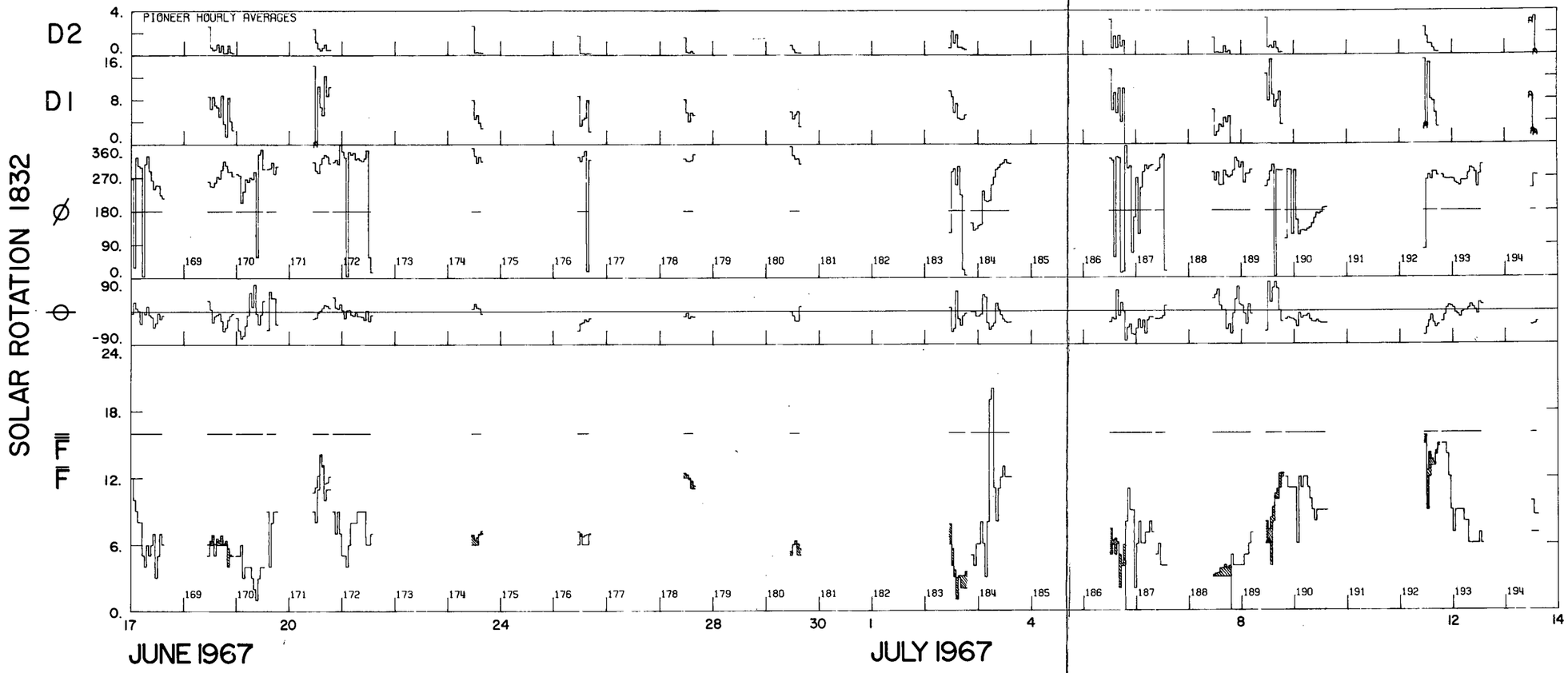

FIGURE 20

FOLDOUT FRAME 1

FOLDOUT FRAME 2

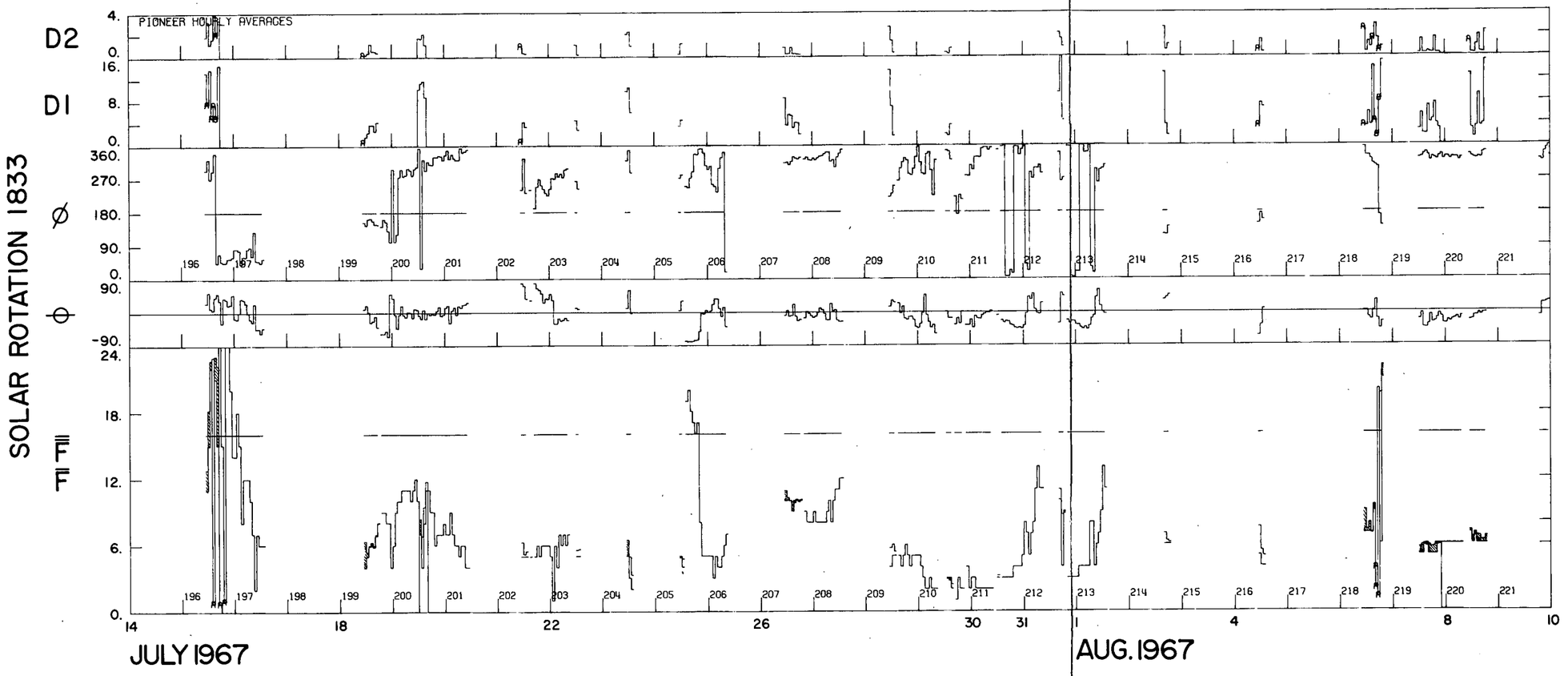

FIGURE 21

FOLDOUT FRAME 1

FOLDOUT FRAME 2

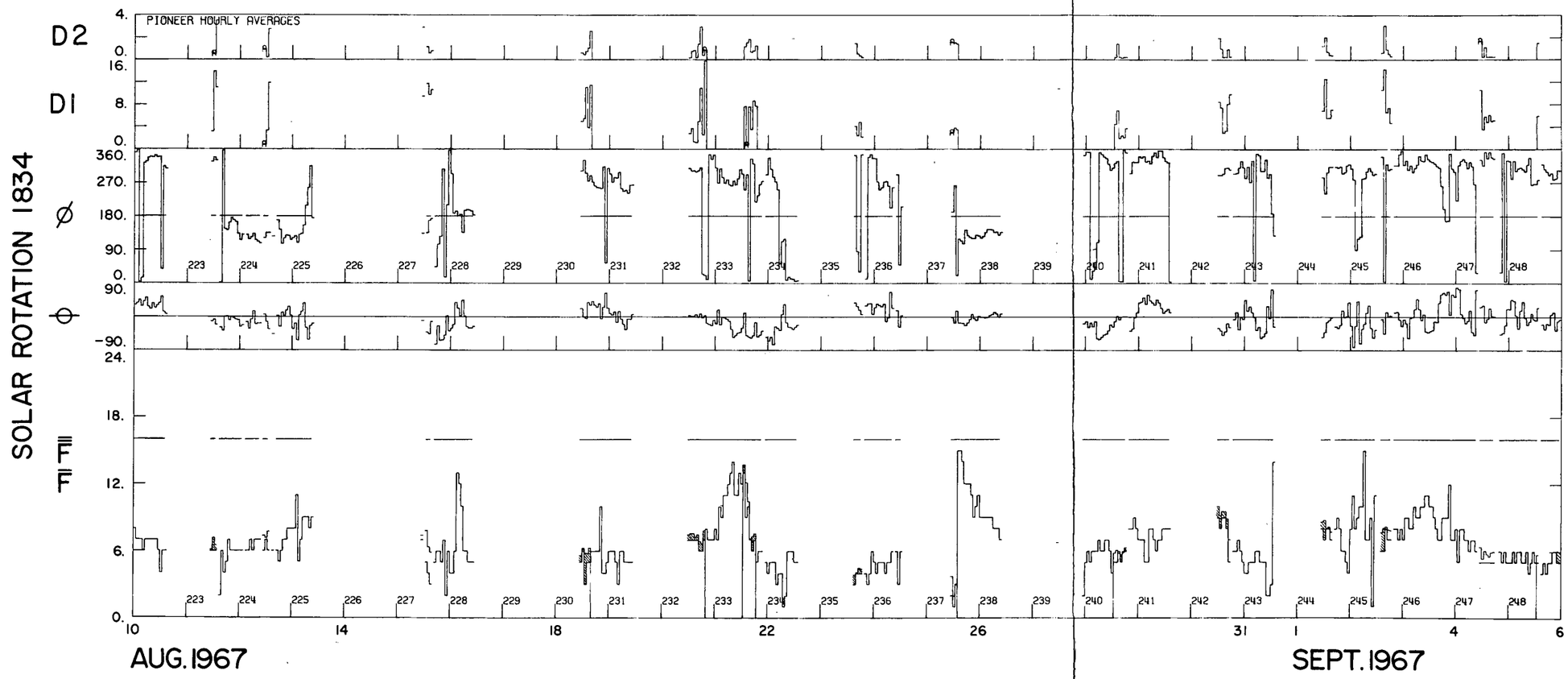

FIGURE 22